Biochemical and Crystallographic Analyses of Maltohexaose-Producing Amylase from Alkalophilic *Bacillus* sp. 707†

Ryuta Kanai,‡,§ Keiko Haga,‡ Toshihiko Akiba,§ Kunio Yamane,‡,|| and Kazuaki Harata*,§

Institute of Biological Sciences, University of Tsukuba, Tsukuba, Ibaraki 305-8572, Japan, and Biological Information Research Center, National Institute of Advanced Industrial Science and Technology, Tsukuba, Ibaraki 305-8566, Japan

Received July 15, 2004; Revised Manuscript Received August 21, 2004

ABSTRACT: Maltohexaose-producing amylase, called G6-amylase (EC 3.2.1.98), from alkalophilic *Bacillus* sp.707 predominantly produces maltohexaose (G6) from starch and related α-1,4-glucans. To elucidate the reaction mechanism of G6-amylase, the enzyme activities were evaluated and crystal structures were determined for the native enzyme and its complex with pseudo-maltononaose at 2.1 and 1.9 Å resolutions, respectively. The optimal condition for starch-degrading reaction activity was found at 45 °C and pH 8.8, and the enzyme produced G6 in a yield of more than 30% of the total products from short-chain amylose (DP = 17). The crystal structures revealed that Asp236 is a nucleophilic catalyst and Glu266 is a proton donor/acceptor. Pseudo-maltononaose occupies subsites −6 to +3 and induces the conformational change of Glu266 and Asp333 to form a salt linkage with the N-glycosidic amino group and a hydrogen bond with secondary hydroxyl groups of the cyclitol residue bound to subsite −1, respectively. The indole moiety of Trp140 is stacked on the cyclitol and 4-amino-6-deoxyglucose residues located at subsites −6 and −5 within a 4 Å distance. Such a face-to-face short contact may regulate the disposition of the glucosyl residue at subsite −6 and would govern the product specificity for G6 production.

Some bacterial α-amylases dominantly produce maltotetraose (G4),[1] maltopentaose (G5), or maltohexaose (G6) from starch and related α-1,4-glucans, while most α-amylases further convert them to glucose and/or maltose as final products. Since such maltooligosaccharides are useful for their low sweetness, low viscosity, high moisturizing effect, and high efficiency for digestion and absorption, they have been important enzymes in the food and pharmaceutical industries.

The reaction mechanism of the enzymes producing particular oligosaccharides is distinct from that of the usual α-amylases. Their important properties are presumed to have four, five, or six subsites from the active center to produce the particular oligosaccharides and to prevent them from further degradation. G4-amlyase (maltotetraose-forming *exo*-amylase) from *Pseudomonas stutzeri* converts short-chain amylose (DP = 23) to G4 in a yield of about 75% (w/w) of the total products and cleaves oligosaccharides G5−G9 to G4 and G1−G3 (*1*). The crystal structure of mutant G4-amylase complexed with maltotetraose has shown that G4-amylase has four subsites at the nonreducing side and binds the glucosyl residue with several hydrogen bonds at subsite −1 (*2*). Furthermore, the glucosyl residue is strongly bound to subsite −4 by hydrogen bonds with Asp160, whereas there are a few contacts between the glucosyl residues and subsites −3 and −2 (*2*). The structure of the sugar binding of G4-amylase suggested that a dominant production of a particular oligosaccharide requires regulated and strong interaction between the subsite and the glucosyl residue of the nonreducing end of the produced oligosaccharide.

G6-amylase (maltohexaose-producing amylase, E.C. 3.2.1.98) from alkalophilic *Bacillus* sp.707, which belongs to glycoside hydrolase family 13 (*3*), has been cloned, and its DNA sequence was determined in 1988 (*4*). Its amino acid sequence is 65.5%, 65.9%, and 66.3% identical to those of liquefying α-amylases from *Bacillus amyloliquefaciens* (BAA), *Bacillus licheniformis* (BLA), and *Bacillus stearothermophilus* (BSTA), but is little homologous to bacterial saccharifying α-amylases and G4-amylase (*4*). Therefore, G6-amylase is presumed to have a structural property different from that of G4-amylase. Many plant α-amylases are also known to temporarily produce maltohexaose from starch (*5*−*7*). The crystal structure of barley α-amylase 2 has been determined (*8*), and the structure of its maltodecaose complex generated by the docking simulation indicated the importance of the stack interaction of Tyr104 with a glucosyl residue bound to subsite −6 to produce maltohexaose (*9*). Therefore, G6-amylase has been expected to have at least six subsites at the nonreducing end and a specific interaction of subsite −6 with a sugar residue.

In this paper, we report the biochemical analysis of G6-amylase from alkalophilic *Bacillus* sp.707 and the crystal structures of the native enzyme and its complex with pseudo-maltononaose (Figure 1) and discuss the mechanism of maltohexaose production.

† This work was supported in part by New Energy and Industrial Technology Development Organization (NEDO) and Grants-in-Aid from the Ministry of Education, Science, Sports, Culture and Technology, Japan.

* To whom correspondence should be addressed. E-mail: k-harata@aist.go.jp. Phone/fax: +82-298-61-6194/3444.

‡ University of Tsukuba.

§ National Institute of Advanced Industrial Science and Technology.

|| Current address. National Food Research Institute, 2-1-12 Kannondai, Tsukuba, Ibaraki 305-8642, Japan.

[1] Abbreviations: Acv, acarviosine unit in acarbose and the pseudo-maltononaose; DP, distribution of polymerization; G1, glucose; G2, maltose; G3, maltotriose; G4, maltotetraose; G5, maltopentaose; G6, maltohexaose; G7, maltoheptaose; G8, maltooctaose; G9, maltononaose; HPLC, high-performance liquid chromatography; TLC, thin-layer chromatography.

10.1021/bi048489m CCC: $27.50
Published on Web 10/05/2004

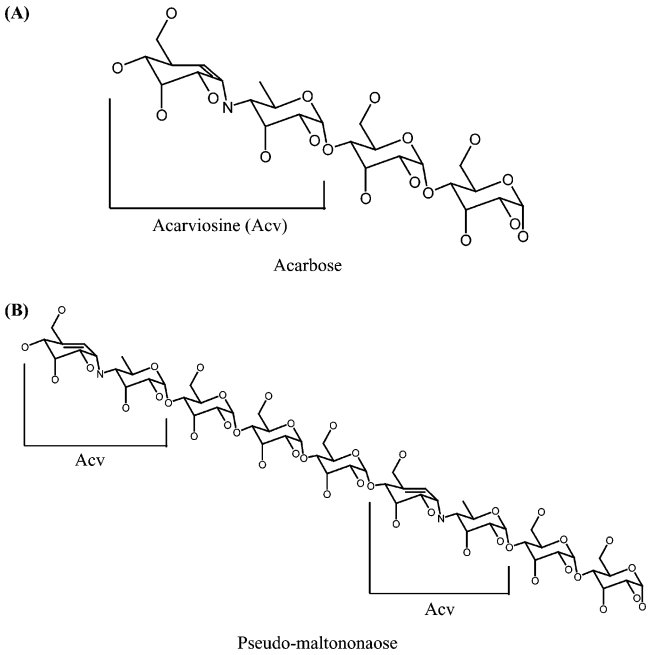

FIGURE 1: Structure of acarbose (A) and pseudo-maltononaose (B) observed in the crystal structure of the G6-amylase complex.

MATERIALS AND METHODS

Chemicals. Kanamycin was purchased from Wako Pure Chemical Industry Ltd. Soluble starch was from E. Merck. Short-chain amylose EX-I (DP = 17), which contains no oligosaccharides (G1−G8), was from Hayashibara Biochemical Laboratories, Inc. Oligosaccharides G1−G7 were from Seikagaku Co. Acarbose was a gift from Drs. A. Mullen and K. Hornberg (Bayer AG). All other chemicals were of reagent grade.

Bacterial Strains and Plasmids. G6-amylase was produced by the transformant of *Bacillus subtilis* 207-25 [m_{168}^- *hsrM recE4 amyE07 aroI906 leuA8 lys-21*] (*10*). Plasmid pTUB812 encodes the G6-amylase gene region of alkalophilic *Bacillus* sp. 707 and has the kanamycin-resistance genes (*10*).

Expression and Purification of G6-Amylase. G6-amylase from alkalophilic *Bacillus* sp. 707 was expressed by the *B. subtilis* 207-25 transformant containing the plasmid pTUB812 as described previously (*10*). The cells were incubated in 6 L of Luria−Bertani medium containing kanamycin (10 μg/mL) and 0.2% (w/v) glucose for 3 days at 37 °C. After 28% saturated ammonium sulfate precipitation of the incubation medium, the supernatant was loaded onto a TOYOPEARL HW55-F (2.5 × 20 cm column size, Tosoh) equilibrated with 28% saturated ammonium sulfate−10 mM sodium phosphate buffer (pH 6.0). The resin was washed, and then the target proteins were eluted with a 28% to 0% reverse gradient of ammonium sulfate. After 75% saturated ammonium sulfate precipitation, the protein was desalted over a Bio-Gel P6-DG column (2.5 × 50 cm column size, BioRad) equilibrated with Milli-Q water and concentrated to 7.0 mg/mL by using an Amicon concentration kit for crystal preparation. In addition, for use in biochemical experiments, the protein was loaded onto DEAE-Sepharose (1.6 × 2.5 cm column size, Pharmacia) equilibrated with 10 mM Tris−HCl buffer (pH7.5) and eluted with a linear 0−500 mM gradient of sodium chloride. The protein was desalted by a HiTrap desalting column (Pharmacia) equilibrated with Milli-Q water and concentrated to 0.48 mg/mL. The purity was over 99% according to SDS−PAGE. The protein concentration was determined using the BCA protein assay reagent (Pierce) with bovine serum albumin as the standard.

Enzyme Assays. Starch-degrading activities were routinely measured at 37 °C in the analysis of pH optima, stability, and thermostability by the blue value method with slight modification (*11*) using a 0.9 mL reaction mixture that contained 0.6 mL of 0.5% (w/v) soluble starch and 0.3 mL of enzyme solution (150−270 ng/mL) finally containing 10 μg/mL bovine serum albumin suitably diluted with Milli-Q water, Britton−Robinson pH buffer (*11*), or 12 mM sodium chloride−50 mM sodium borate buffer (pH 8.8). After preincubation for 5 min and incubation for 5, 10, and 15 min, the reaction was halted and the starch was colored by adding stop solution (0.17 mM I_2, 1.7 mM KI, and 1.7 mM HCl). One unit of starch-degrading activity was defined as the amount that generated a 1% decrease in absorbance at 660 nm/min. The pH optima were determined by diluting enzyme solution with each Britton−Robinson pH buffer as described previously (*11*). The pH stability was examined by maintaining the various pH values of each enzyme solution for 30 min at 37 °C before adjustment to pH 8.8 with 12.5 mM sodium chloride−50 mM sodium borate buffer. In the assay of thermostability, an enzyme solution suitably diluted by the sodium borate buffer (pH 8.8) was left for 30 min at various temperatures and preincubated at 37 °C after being cooled in ice−water for 5 min. In the assay of optimal temperature, each enzyme solution diluted by the sodium borate buffer (pH 8.8) was preincubated at various temperatures and the activity at various temperatures was measured as described above.

Analysis of Reaction Products. Reaction proceeded at 40 °C in a 1.2 mL reaction mixture that contained 0.8 mL of 1.0% (w/v) amylose EX-I (DP = 17) solution and 0.4 mL of an enzyme solution (final 1 or 40 U/mg of amylose) diluted with sodium borate buffer (pH 8.8). After sampling of a 0.1 mL reaction mixture, the enzyme reaction at various reaction times was stopped by boiling for 10 min. The products were quantified using HPLC. After desalting of the samples and filtration through a 0.22 μm pore membrane, the reaction products were eluted from a LiChrosorb NH_2 column (25 × 0.4 cm column size, Cica-Merck) equilibrated with 68% (v/v) acetonitrile at a flow rate of 0.8 mL/min and detected using the differential refractometer detector RI-71 (Shodex). The products G1−G7 were quantified by comparison with each linear calibration G1−G7 curve of standard.

Reaction Pattern Using G5, G6, and G7. All reactions proceeded at 40 °C in reaction mixtures of 60 μL containing 20 mM G5, G6, or G7 and 240 μL of the enzyme (final concentration 8 U/μmol of substrate) in the sodium borate buffer (pH 8.8). After incubation for 10, 20, and 30 min, the reactions were stopped by boiling for 10 min. The reaction products were analyzed by using TLC. The loaded samples were developed in a solution of 2-propanol/ethyl acetate/water (3:1:1, v/v/v) for 1 h by TLC plates (silica gel 60 F_{254}, 5 × 7.5 cm plates (Merck)) and dried. After this procedure was repeated three times, all carbohydrates were visualized by spraying the plates with 20% (v/v) sulfuric acid in ethanol and baking at 120 °C.

Crystallization of Native G6-Amylase and Its Complex with Pseudo-Maltononaose. G6-amylase was crystallized by the

Table 1: Statistics of Diffraction Data and Structure Determination

	native	complex
Diffraction Data		
space group	orthorhombic $P2_12_12_1$	orthorhombic $P2_12_12_1$
unit cell parameters (α, β, γ (Å))	47.62, 82.80, 127.18	47.41, 82.49, 126.88
V_M	2.26	2.10
mosaicity	0.664	0.315
resolution range (last shell) (Å)	50.0−2.04 (2.11−2.04)	50.0−1.94 (2.01−1.94)
total no. of reflections	123734	271436
no. of unique reflections	32772	39906
completeness (last shell) (%)	99.6 (97.8)	98.8 (98.8)
R_{merge} (last shell) (%)	9.1 (24.8)	5.1 (10.6)
redundancy	2.60	3.40
Structure Determination		
resolution range (last shell) (Å)	6.0−2.1 (2.17−2.10)	6.0−1.9 (1.98−1.94)
no. of reflections used ($>2\sigma$)	26098	36914
completeness (last shell) (%)	90.8 (79.5)	95.4 (83.3)
protein	5−485 (1−4 disordered)	5−485 (1−4 disordered)
no. of water molecules	282	324
final R value (last shell) (%)	16.6 (17.7)	17.2 (18.4)
final R_{free} value (last shell) (%)	21.0 (23.2)	20.7 (24.5)
RMSD		
bond length (Å)	0.005	0.005
bond angle (deg)	1.28	1.24
dihedral angle (deg)	23.48	23.56
improper angle (deg)	0.688	0.732

hanging drop vapor diffusion method using a reservoir solution containing 50% (v/v) 2-methylpentane-2,4-diol, 100 mM Tris−HCl (pH 8.5), and 200 mM ammonium phosphate. A drop solution contained equal volumes of sample and reservoir solutions, and then calcium chloride and sodium chloride were added to a final 1 mM concentration in the drop solution. Rodlike crystals of $0.3 \times 0.1 \times 0.05$ mm^3 were developed within 4 days at room temperature. Crystals of the complex with pseudo-maltononaose were obtained by soaking for 3 days in the crystallization solution containing 10 mM acarbose (Figure 1) and 10 mM maltotriose.

Measurement of Diffraction Data. The X-ray diffraction data of the crystals of the native enzyme and its complex with pseudo-maltononaose were collected to 1.94 Å resolution at 100 K at the BL-6A and AR-NW12 stations of the Photon Factory, respectively, and processed using the program HKL2000 (*12*). Sugar complex crystals were isomorphous with the native crystal. Statistics of the data collection are summarized in Table 1.

Structure Determination and Refinement. All the calculations in the structure determination and refinement were performed by using the program CNS (*13*). The crystal structure of the native G6-amyalse at 2.1 Å resolution was determined by molecular replacement using a set of coordinates of a mutant α-amylase from *B. licheniformis* (PBD code 1OB0) (*14*) as the starting model. The amino acid sequence was manually corrected using the program TURBO-FRODO on the $|3F_o - 2F_c|$ and $|F_o - F_c|$ electron density maps, and three calcium, one sodium, phosphate, and Tris ions were located. Water molecules were picked up using CNS (*13*), but those with a B factor over 60 Å^2 were omitted during the refinement.

The crystal structure of the G6-amylase complex with pseudo-maltononaose was determined by molecular replacement using the native structure and refined at 1.9 Å resolution. The $|3F_o - 2F_c|$ and $|F_o - F_c|$ electron density maps clearly showed pseudo-maltononaose located at subsites −6 to +3. The sugar molecule was initially constructed as an α-1,4-linked chain of nine 6-deoxy-D-glucoses, and then the structure was corrected to Acv-Glc-Glc-Glc-Acv-Glc-Glc (Acv = acarviosine, a disaccharide analogue unit in pseudo-maltononaose; Glc = glucose) (Figure 1) on the electron density maps. The stereochemical qualities of the structures were checked by the program PROCHECK (*15*). Statistics of the structure determination are summarized in Table 1. Atomic coordinates have been deposited with the Protein Data Bank (native structure, 1WP6; complex structure, 1WPC).

Theoretical Calculation of ΔpK_a *Values.* The ΔpK_a value was calculated using the program DELPHI (*16*) for a finite difference solution to the nonlinear Poisson−Boltzmann equation. The electrostatic potential was calculated with formal charges, a grid size of $0.3 \times 0.3 \times 0.3$ Å^3, an ionic strength of 0.145 M, and interior and external dielectric constants of 2.0 and 80.0, respectively. The ΔpK_a value of the target residue was calculated by the equation

$$\Delta pK_a = \frac{\sum \phi_n q_n}{2.303}$$

where ϕ_n is the electrostatic potential of the other atom n induced by the charge of the target residue and q_n is the formal charge (*17*).

RESULTS

The culture medium after incubation for 3 days had a starch-degrading activity of about 700 U/mL at pH 7.6, and the purity of G6-amylase after TOYOPEARL HW-55F chromatography treatment was about 95%. Moreover, the final purity after DEAE-Sepharose chromatography treatment was over 99%. Since the starch-degrading activity of the purified G6-amylase was 15000 U/mg at pH 7.6, the yield of G6-amylase by *B. subtilis* 207-25 was estimated to be 46 mg/L of culture medium.

Enzyme Assays. Analysis of the pH optima for the starch-degrading activity showed that the activity of G6-amylase was maximal (18800 U/mg) at pH 8.8 and retained a relative activity higher than 50% between pH 6.5 and pH 10.0 (Figure 2A). The pH stability was measured by the starch-degrading activity at pH 8.8 after each enzyme was incubated at various pH values for 30 min at 37 °C. The enzyme was more than 50% stable in the pH range from 4.7 to 10.8 (Figure 2B). The optimal temperature of G6-amylase was 45 °C at pH 8.8, and the enzymatic activity decreased to less than 20% at temperatures above 70 °C (Figure 2C). The thermostability was measured as starch-degrading activity at 37 °C after each enzyme was incubated at various temperatures for 30 min. The enzyme retained a stability of more than 90% at 45 °C, but the stability decreased to below 20% at temperatures over 55 °C (Figure 2D). The amino acid sequence of G6-amylase is about 65% identical to those of BLA and BSTA (*4*), but its optimal temperature was lower than those of BLA and BSTA (*18*, *19*).

Product Ratios of Maltooligosaccharides from Short-Chain Amylose. At a low concentration (1 U of enzyme/mg of amylose) of G6-amylase (Figure 3A), the production rates

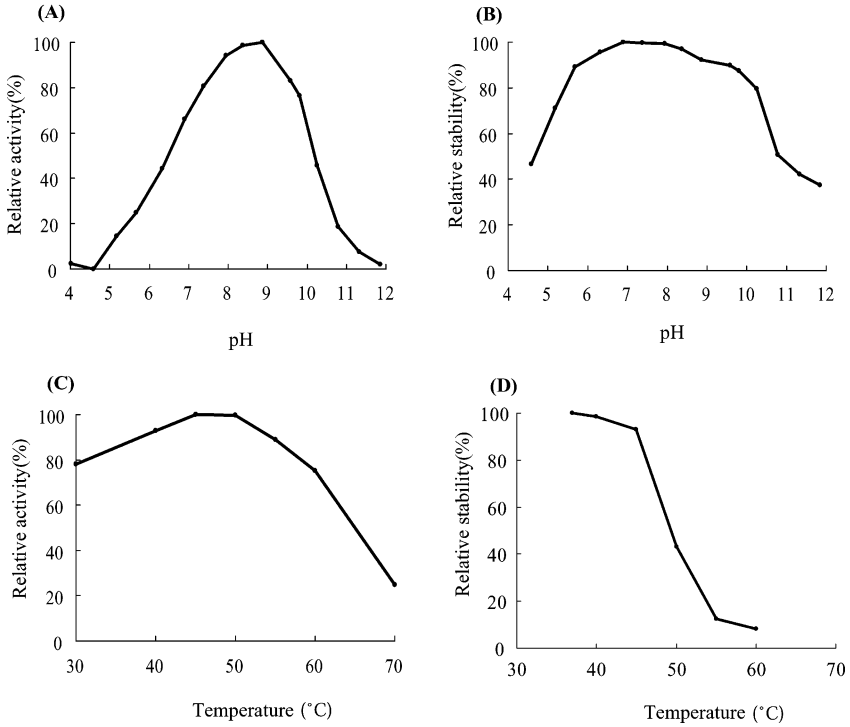

FIGURE 2: Characterization of *Bacillus* sp. 707 G6-amylase for starch-degrading activity. Effects of pH and temperature on its activity (A, C) and stability (B, D). Assays of pH (A and B) were performed at 37 °C, and temperature assays (C and D) were performed in 50 mM sodium borate−12.5 mM sodium chloride buffer (pH 8.8).

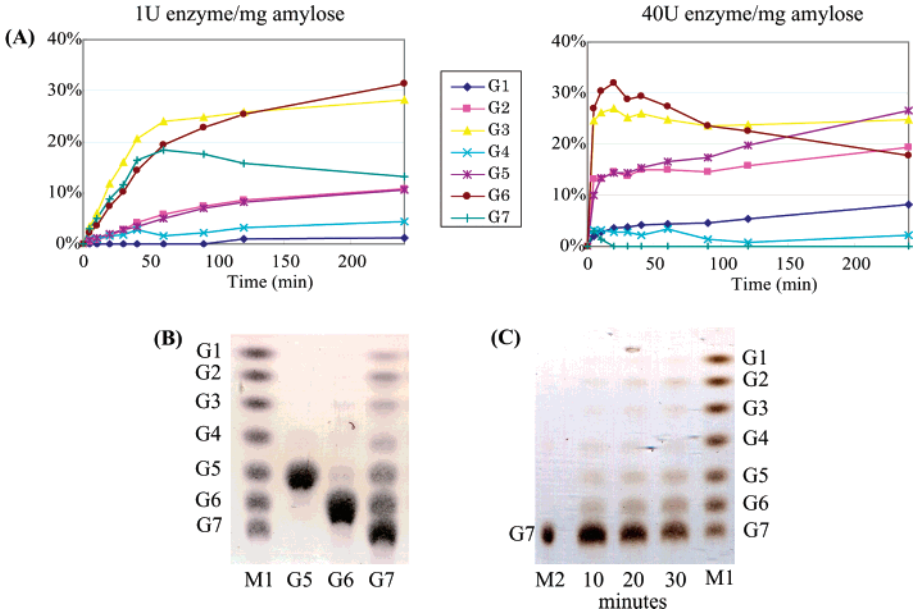

FIGURE 3: Product ratio of short-chain amylose (DP = 17) and cleavage pattern profile of G5, G6, and G7. (A) The product ratio of short amylose (DP = 17) was determined by HPLC analysis. The amount of the enzyme was 1 (right) and 40 (left) U of enzyme/mg of amylose. (B) TLC analysis of the degradation pattern of G5, G6, and G7 after 30 min of incubation. (C) TLC analysis of the degradation pattern of G7 after 10, 20, and 30 min of incubation. M1 and M2 are markers of G1−G7 and G7, respectively.

(% (w/w) total sugar/min) of G3, G6, and G7 were 0.49 (50.2 μM/min), 0.35 (18.1 μM/min), and 0.37 (16.5 μM/min), respectively, in 40 min. The amount of G3 in total sugar reached 24−28% (w/w) (2.5−2.9 mM) in 90 min and was constant over the next 24 h. The production of G6 slowly increased to 31.4% (1.6 mM) in 240 min and then remained essentially constant over the next 24 h. The highest product ratio of G7 was 18.4%, which was obtained after 60 min, but this decreased to 0% after 24 h. With high concentrations of G6-amylase (40 U/mg of amylose), the levels of G3 production were about 25% (2.2 mM) throughout the entire reaction period (Figure 3A), while G6 production initially increased to 32.0% (1.4 mM) at 20 min but fell to 0% after 24 h. In contrast, the production of G1, G2, and G5 increased to 13.0% (3.3 mM), 25.0% (3.3 mM), and 35.4% (1.9 mM) after 24 h. The production profiles of 1% (w/w) soluble starch as a substrate with different enzyme concentrations of 1−60 U/mg of substrate were analyzed by using TLC. The profiles of soluble starch with low and high enzyme concentrations (1−4 and 20−60 U/mg of substrate) were similar to those

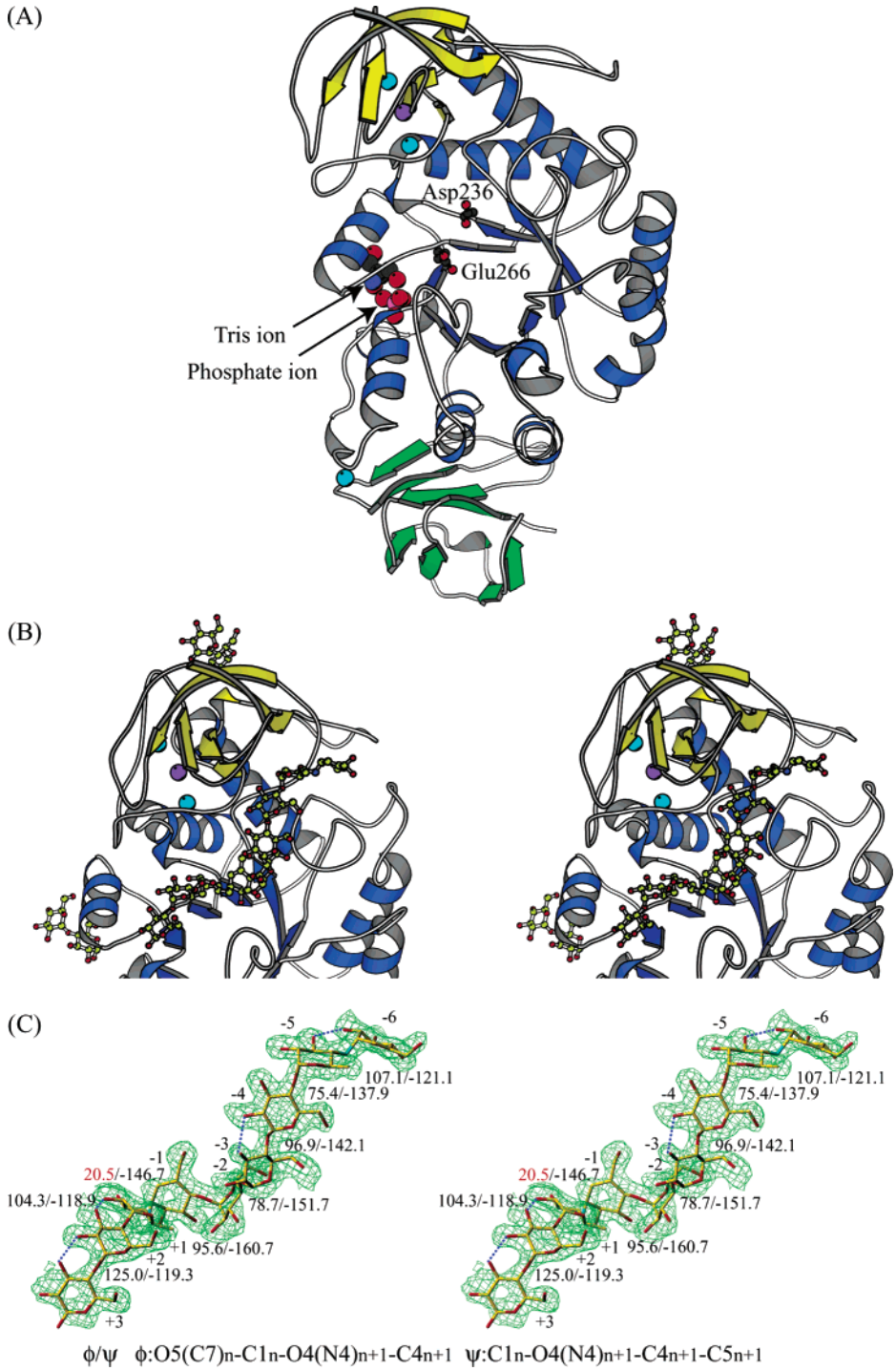

FIGURE 4: Crystal structures of G6-amylase from alkalophilic *Bacillus* sp. 707. (A) G6-amylase is composed of three domains, A (blue), B (yellow), and C (green). Asp236 as a nucleophilic catalyst and Glu266 as a proton donor/acceptor are represented by balls and sticks. Three calcium ions and one sodium ion are shown as cyan and purple spheres, respectively. (B) Crystal structure of the G6-amylase complex with pseudo-maltononaose. Sugar molecules are represented by balls and sticks. (C) Structure of pseudo-maltononaose with an omit $|F_o - F_c|$ electron density map at the 1.5σ level. Torsion (ϕ, ψ) angles of glycosidic bonds are given, and intramolecular hydrogen bonds are represented by broken lines.

of short-chain amylose (DP = 17) with enzyme concentrations of 1 and 40 U/mg of amylose, respectively (data not shown).

Reaction Products of G5, G6, and G7. The TLC analysis of the products for 4 mM G5 and G6 as substrates in the presence of G6-amylase (8 U/μmol of substrate) showed that G6-amylase is inactive toward G5 and is slightly converted to G5 (Figure 3B). In contrast, the enzyme produced all of G1−G6 from G7 (Figure 3C) although G7 was mostly cleaved to G5 and G2 or G6 and G1, as shown by the relatively dense spots for these products.

Crystal Structure of Native G6-Amylase at 2.1 Å Resolution. G6-Amylase consists of three domains, A, B, and C (Figure 4A). Domain A (5−105, 208−396) forms a $(\beta/\alpha)_8$ barrel like the other enzymes of the α-amylase family. Domain B (106−207) is composed of six β-strands and loops, and two long β-strands form a wound β-sheet fold. A *cis*-peptide bond is observed between Trp189 and Glu190.

Domain C (397−485) consists of eight β-strands and some loops as observed in the other α-amylases (*2*, *20*, *21*).

The backbone structure of G6-amylse is similar to those of liquefying α-amylases BLA (*21*) and BSTA (*22*) with an average difference in their equivalent Cα position of less than 1.0 Å. The relatively large difference was observed in regions 172−177, 181−185, 311−316, and 373−380. Except for region 311−316, these regions involve a deletion or insertion of some amino acid residues. G6-Amylase like BLA (*21*) and BSTA (*22*) contains the $Ca^{2+}-Na^{+}-Ca^{2+}$ metal ion triad at the interface between domain A and domain B. The side chains of six aspartic acids (Asp163, Asp188, Asp199, Asp205, Asp207, and Asp209), one asparagine (Asn106), three backbone carbonyl groups, and two water molecules are coordinated to the three metal ions. Compared with the other enzymes of the α-amylase family (glycoside hydrolase family 13 (*3*)), bacterial saccharifying α-amylase (*23*), barley α-amylase (*8*), G4-amylase (*2*), and maltogenic amylase (*24*), the structures of domains A and C of G6-amylase are similar to their corresponding domains but that of domain B considerably differs.

A structural comparison with the other enzymes of the α-amylase family indicates that Asp236 is a nucleophilic catalyst and Glu266 is a proton donor/acceptor catalyst. The conformations of amino acid residues Tyr58, Asp102, Lys239, His240, His332, and Asp333 around the catalytic residues conserved in many α-amylases are similar to those observed in other α-amylases (*2*, *8*, *20*−*25*).

Crystal Structure of G6-Amylase Complexed with Pseudo-Maltononaose. The pseudo-maltononaose molecule is bound at subsites −6 to +3 of G6-amylase like an enzyme−substrate complex (Figure 4B). The structure of pseudo-maltononaose, Acv-Glc-Glc-Glc-Acv-Glc-Glc (Figure 4C), suggests that it is derived from acarboses and maltotrioses by intermolecular transglycosylation and hydrolysis. In many crystals of α-amylase complexes with acarbose as reported previously, acarbose molecules are converted to an oligosaccharide that inhibits the enzyme activity more effectively (*26*−*29*).

Conformation of Pseudo-Maltononaose. Intramolecular hydrogen bonds linking $O2H_n$ and $O3H_{n+1}$ hydroxyl groups are observed between the glycosyl residues at subsites −6/−5, −4/−3, +1/+2, and +2/+3 (Figure 4C). Torsion angles (ϕ, $O5(C7)_n-C1_n-O4(N4)_{n+1}-C4_{n+1}$; ψ, $C1_n-O4(N4)_{n+1}-C4_{n+1}-C5_{n+1}$) of glycosidic linkages, ϕ angles of 75.4−125.0° and ψ angles of −160.7° to −118.9°, are in the energetically favored region except for the ϕ angle at subsite −1/+1 of 20.5° (Figure 4C). Half-chair forms are observed in two cyclitol residues at subsites −6 and −1 (Figure 4C).

Contacts between Pseudo-Maltononaose and G6-Amylase. Many hydrogen bonds are observed between the cyclitol or glycosyl residues and amino acid residues Tyr198, Glu194, Arg234, Asp236, Lys239, His240, Glu266, His332, and Asp333 located at subsites −1 to +2 (Table 2 and Figure 5A). The carboxyl group of the nucleophile Asp236 is close to the C1 atom of the cyclitol residue at subsite −1 at a 3.1 Å distance, and the side chain of Glu266, a proton donor/acceptor catalyst, has a close contact at a 2.8 Å distance to a nitrogen atom of the N-glycosidic bond between the cyclitol and 4-amino-6-deoxyglucosyl residues at subsites −1 and +1 (Table 2 and Figure 5B). Such close contacts of catalytic residues have also been found in many other α-amylase complexes reported previously (*24*, *26*−*28*). Moreover, the aromatic ring of Tyr58 is parallel to the pyranose ring of the cyclitol residue at subsite −1 within a 4 Å distance (Figure 5A), indicating the hydrophobic stack as observed in many α-amylase−carbohydrate complexes (*2*, *23*, *24*, *26*−*28*).

Table 2: List of Short Contacts (≤3.3 Å Distance) of Pseudo-Maltononaose to G6-Amylase

sugar		protein	distance (Å)	sugar		protein	distance (Å)
−6	O2	Ala111N	3.3	−1	C1	Asp236Oδ1	3.1
		Ala111O	2.8		O2	Arg234NH2	3.0
	O3	Lys72Nζ	2.9			His332Nε2	2.8
−5	O2	Wat734	2.9			Asp333Oδ2	2.3
		Wat735	2.6			Wat708	3.3
	O3	Gly110N	3.2		O3	His332Nε2	3.1
		Ala111N	3.1			Asp333Oδ1	2.7
	N4	Wat733	3.1			Asp333Oδ2	3.3
−4	O2	Asp166Oδ2	2.5		O6	Asp236Oδ2	2.7
		Tyr203N	3.1		C7	Asp236Oδ1	3.1
	O3	Asp166Oδ1	2.6	+1	O2	His240Nε2	2.6
		Tyr203N	3.3		O3	Glu266Oε1	3.1
		Wat734	2.9			Glu266Oε2	2.7
−3	O2	Wat858	3.1		N4	Glu266Oε1	2.8
		Wat862	2.7			Asp333Oδ2	3.1
	O3	Wat858	3.1		O5	Wat906	2.7
−2	O2	Asp333Oδ1	3.2	+2	O2	Glu194Oε2	2.6
		Wat707	2.6			Lys239Nζ	2.9
	O3	Wat862	2.6		O3	Tyr198OH	3.2
	O6	Wat704	2.6			Lys239Nζ	2.6
		Wat705	2.9		O6	Wat906	3.0
						Wat986	2.7
				+3	O1	Wat966	3.2
						Wat979	2.5
					O2	Asn270N	2.8

The glucosyl residues at subsites −3 and −2 form only one hydrogen bond with Asp333 but several hydrogen bonds with water molecules (Table 2). The carboxyl group of Asp166 forms strong hydrogen bonds with the O2H and O3H hydroxyl groups of the glucosyl residue at subsite −4 with 2.5 and 2.6 Å distances, respectively, and the aromatic ring of Tyr203 is parallel to the pyranose ring at about a 4 Å distance, indicating the hydrophobic stack. At subsites −6 and −5, in addition to hydrogen bonding by Lys72, Gly110, and Ala111, the aromatic ring of Trp140 closely contacts within a 4 Å distance the C4 atom of the 4-amino-6-deoxyglucosyl residue at subsite −5 and the C1 atom in the cyclitol residue at subsite −6 (Figure 5C). These findings indicate that the hydrophobic stack interaction strictly determines the disposition of these sugar residues at these subsites.

Structural Comparison of Native G6-Amylase with Its Complex. Complex formation caused structural changes in the catalytic active site. In the complex, the carboxyl group of Glu266 no longer forms hydrogen bonds to the side chains of Asp333 and Arg234 (Figure 5B) but moves to the sugar residue with a change of its χ_2 angle from 172.2° to −126.7° to form a hydrogen bond with the O3H hydroxyl group and a salt bridge with the N4 amino group of the 4-amino-6-deoxyglucosyl residue at subsite +1 (Figure 5B). Furthermore, Cα atoms of Asp333 and His332 forming hydrogen bonds to the sugar ligand are shifted by 1.1 and 0.6 Å, respectively, from their position in the native structure (Figure 5A). The calculated ΔpK_a values of the carboxyl group of Glu266 referred to as a proton donor/acceptor catalyst are +17.6 and +4.4 for the native and complex

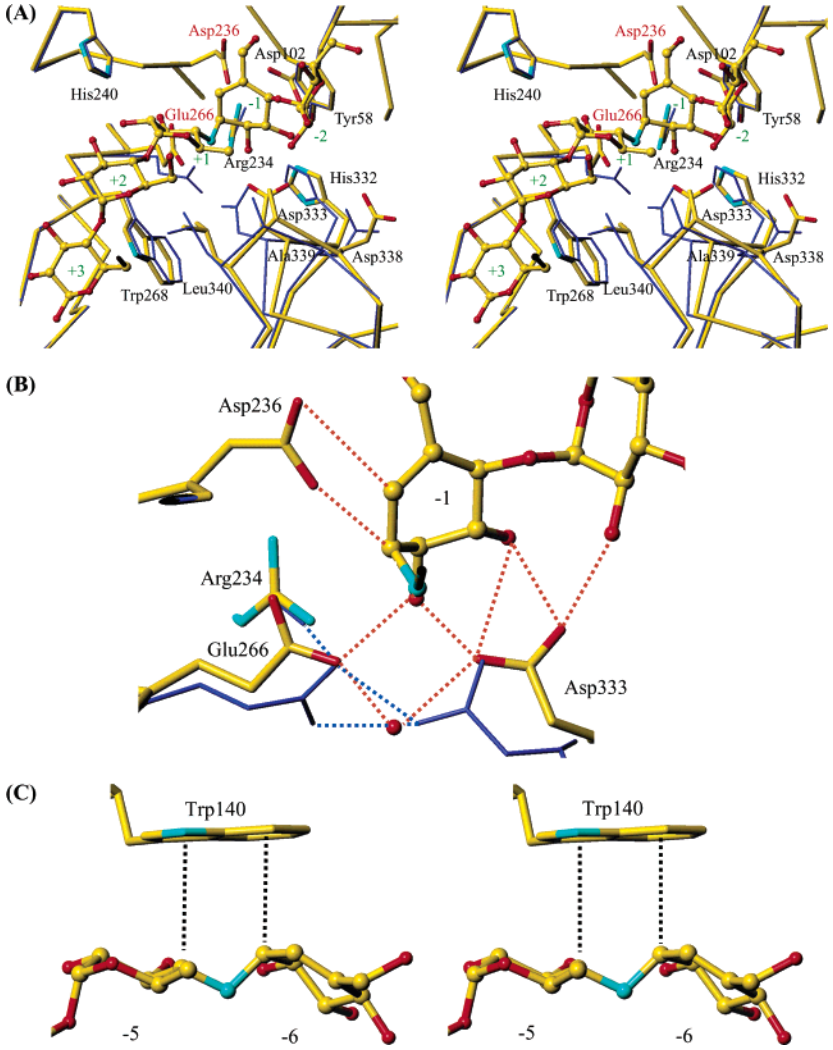

FIGURE 5: Structural change of the active site between the native enzyme (thin purple sticks) and its complex with pseudo-maltononaose (thick sticks). (A) Structural change of subsites −2 to +3. (B) Structural changes of the Asp236 and Glu266 catalytic residues and Asp333. Hydrogen bonds and short contacts (≤3.3 Å) are shown by broken lines. (C) Hydrophobic stacking interaction of the indolyl moiety of Trp140 with the 4-amino-4,6-deoxyglucosyl and cyclitol residues at subsites −5 and −6, respectively.

structures, respectively. The effect of Asp333 on the ΔpK_a of Glu266 is decreased by −10.9 in the complexed state. This indicates that the structural changes of Glu266 and Asp333 cause the change of the electrostatic environment and affect their protonation/deprotonation (Figure 5B), and the ΔpK_a value of Glu266 explains the high activity of the alkalophilic G6-amylase in a basic pH condition.

The Cα atoms of Glu338, Ala339, and Leu340 are respectively moved 1.0, 1.7, and 0.9 Å closer to His332 and Asp333 (Figure 5A). In the structure of the complex, the carbonyl oxygen atom in the backbone of Asp333 forms a hydrogen bond with the backbone peptide group of Leu340 and the Cδ1 atom of Leu340 is close to the aromatic ring of Trp268 within a 4 Å distance (Figure 5A).

DISCUSSION

Crystal Structure of G6-Amylase. The backbone structure of G6-amylase resembles the structure of bacterial liquefying α-amylases BLA (*21*) and BSTA (*22*). The structures of their B domains are considerably different from those of other α-amylases (*2*, *23*, *24*) because the amino acid sequences of the B domains are longer by 20−40 amino acids than those of the other α-amylases. Since BLA produces G5 from starch and related α-1,4-glucans, the structure of domain B of these enzymes may be specific for G5 or G6 production. In fact, Lys72, Trp140, Asp166, and Tyr203 in domain B, which are conserved in BLA (*21*), participate in constructing the subsite structure as described above (Table 2 and Figure 5C).

Structural Changes in G6-Amylase Induced by ES Complex Formation. The movement of Asp333 in the complex with pseudo-maltononaose (Figure 5B) should be induced by substrate binding to optimize the interaction between protein and substrate. Furthermore, since the carboxyl group of Asp333 is expected to decrease the pK_a value of Glu266 in the pseudosubstrate−enzyme complex, the structural changes of Glu266 and Asp333 would be important for efficient catalytic activity. The carboxyl group of Glu266 in the native form may not be ionized even at a high pH environment, but in an ES complex, it would easily release a proton to donate it to the glycosidic oxygen atom at the cleavage site (Figure 5B).

The positional movement of region 338−340 toward region 332−333 may have arisen to relieve the steric hindrance between the side chain of Leu340 and the sugar ligand, and to impose a restriction on the substrate conformation for effective binding. If a structural change does not

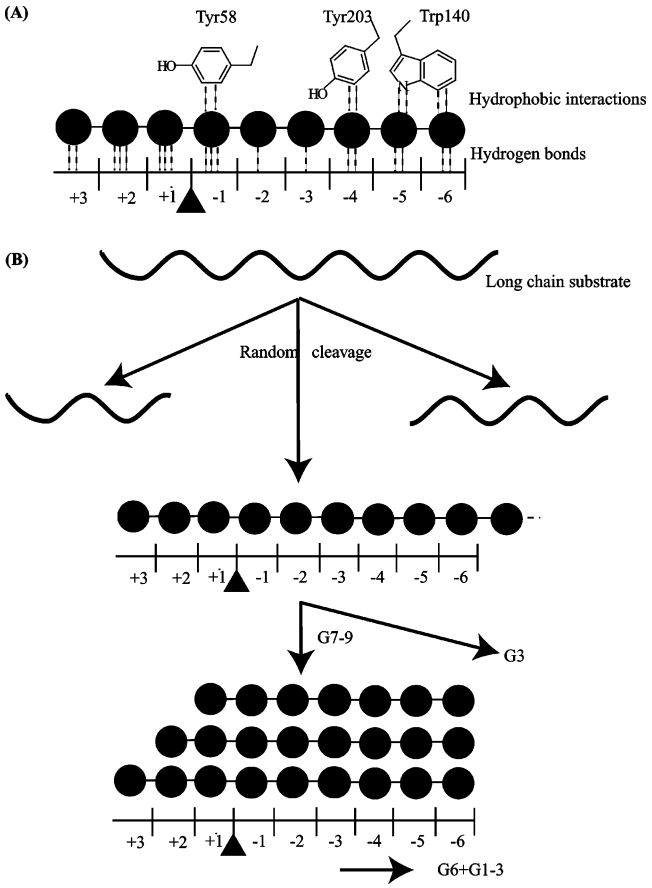

FIGURE 6: Schematic representation of the reaction mechanism of G6-amylase. (A) Characteristic drawing of the interactions of the subsites with substrate. Hydrophobic stacking and hydrogen bonds are shown by broken lines. (B) Proposed reaction process for amylose degradation and G6 production by G6-amylase.

occur, the side chain of Leu340 would be too close within a 3.5 Å distance to the glycosyl residues at subsites +1 and +2 and the side chain of Ala339 would be far from the glucosyl and cyclitol residues at subsites −2 and −1 (Figure 5A). Trp268 may contribute to stabilization of region 338−340 through CH−π interaction with Leu340 (Figure 5A). Regions 332−333 and 338−340 contact each other and are involved in the structural change to accommodate the substrate during ES complex formation. Therefore, the enzyme−substrate interaction would be optimized by such structural changes as described in terms of the induced fitting.

Binding of Oligosaccharide to Subsites. The structure of the pseudosubstrate−enzyme complex indicates that the active site of G6-amylase consists of at least three and six subsites at the reducing and nonreducing ends, respectively (Figure 6A). The many hydrogen bonds at subsites −1 and +1 and the stack interaction of Tyr58 with the cyclitol and 4-amino-6-deoxyglucosyl residues (Table 2 and Figure 5A) indicate that subsites −1 and +1 bind the glucosyl residues tightly enough to distort and cleave the glycosidic bond between the glucosyl residues at these locations.

The glucosyl residues should be tightly bound to subsites −6 and −5 since the aromatic ring of Trp140 is stacked on the cyclitol and 4-amino-6-deoxyglucosyl residues by van der Waals and/or CH−π interactions and they also have hydrogen bonds to amino acid residues in the subsites (Table 2 and Figure 5C). Moreover, the hydrogen bonds of Asp166 and the stacking of the aromatic ring of Tyr203 to the glucosyl residue (Table 2) suggest strong binding of the glucosyl residue to subsite −4. We tried to determine the crystal structures of the enzyme complexed with various maltodextrins, and the electron densities of the glucosyl residues were more visible at subsites −6 to −4 than those at the other subsites (data not shown). Despite the break of the intramolecular hydrogen bonds between secondary hydroxyl groups of the 4-amino-6-deoxyglucosyl and glucosyl residues at subsites −5 and −4 (Figure 4C), their conformation is strictly confined by the interaction with the subsites. In contrast, the few hydrogen-bonding contacts of subsites −3 and −2 to glucosyl residues (Table 2) indicate weak binding of these residues to the subsites. However, the conformations of glucosyl residues at subsites −3 and −2 are restricted by van deer Waals interaction with region 338−340 (Figure 5A).

Amylose Degradation and Maltohexaose Production of G6-Amylase. Since the analysis of the product ratio of short-chain amylose showed high production levels (about 25% total sugar) of G3 during the early stages of hydrolysis, a substrate, Gn ($n \geq 9$), may occupy subsites from +3 toward the nonreducing end of the active site and be hydrolyzed to G3 and Gn−3 (Figure 6B). If such a binding mode of the substrates is dominant, the enzyme would produce mostly G3 from oligomaltoside in a fashion similar to that of BLA acting on G8, G9, or G10 (*30*). However, the X-ray structure shows that there is no structural "barrier" preventing the binding of more than three sugar residues at the reducing end. Therefore, the hydrolysis to G3 and Gn−3 by G6-amylase would be followed by the random cleavage of a long-chain substrate. When amylose is degraded to produce G7, G8, or G9, these substrates may be accommodated to occupy six subsites at the nonreducing end and hydrolyzed to G6 and G1 or G2 or G3 (Figure 6B). The interaction of subsites −6 and −5, especially Trp140, with the glucosyl residues would play an important role in G6 production. The powerful interaction of subsite −6 with the glucosyl residue indicates a possibility to form nonproductive binding (enzyme−product complex) of G6 that occupies subsites −6 to −1 since the electron density map of the X-ray structure acquired by soaking G6-amylase crystals in a solution with a high concentration of maltohexaose showed a sugar chain occupying subsites −6 to −2 (data not shown).

Importance of an Aromatic Residue at Subsite −6 on Maltohexaose Production. Barley α-amylase temporarily produces maltohexaose from starch but finally hydrolyzes it to glucose and/or maltose (*31*). The structural model of a barley α-amylase−ligand complex, which is obtained by superimposing the pseudo-maltononaose structure in the G6-amylase complex at the equivalent location of the native structure of barley α-amylase 2 (*8*), shows that, despite the low sequence similarity, the location of Tyr104 is almost identical to that of Trp140 at subsite −6 of G6-amylase (Figure 7). This structural similarity of subsite −6 indicates the importance of the interaction of an aromatic residue at subsite −6 with a glucosyl residue in maltohexaose production. The recent biochemical analysis of subsite −6 of barley α-amylase 1 has shown that replacing Tyr105 with alanine causes low degradation activity and changes the cleavage pattern profile of PNP-G7 (*32*). At present, we are examining the importance of Trp140 on maltohexaose production using site-directed mutagenesis and a biochemical approach.

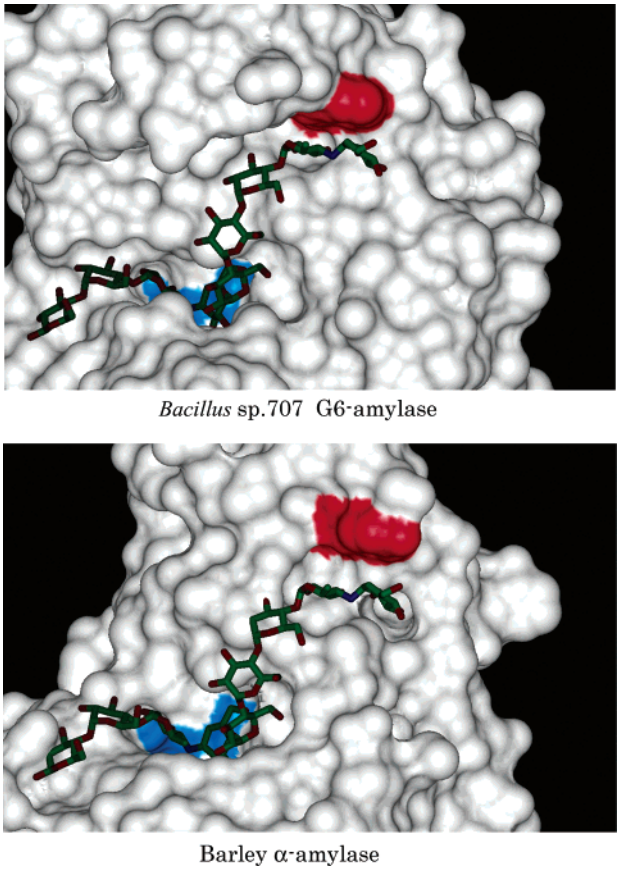

FIGURE 7: Binding of pseudo-maltononaose with G6-amylase (upper) and barley α-amylase 2 (lower). The complex structure of barley α-amylase 2 with pseudo-maltononaose was modeled by the superimposition of the ligand on the position in its native structure (*8*) equivalent to that of G6-amylase. The catalytic residues and the aromatic residue at subsite −6 are colored cyan and red, respectively.

ACKNOWLEDGMENT

We thank Drs. A. Mullen and K. Hornberg for supplying acarbose, Drs. M. Suzuki, N. Igarashi, and N. Matsugaki of the Photon Factory, High Energy Accelerator Research Organization, for their help in data collection using synchrotron radiation. We also thank N. Foster for critically reading the manuscript.

REFERENCES

1. Nakakuki, T., Azuma, K., and Kainuma, K. (1984) Action patterns of various exo-amylases and the anomeric configurations of their products, *Carbohydr. Res. 128*, 297−310.
2. Yoshioka, Y., Hasegawa, K., Matsuura, Y., Katsube, Y., and Kubota, M. (1997) Crystal structures of a mutant maltotetraose-forming exo-amylase cocrystallized with maltopentaose, *J. Mol. Biol. 271*, 619−628.
3. Henrissat, B., and Davies, G. (1997) Structural and sequence-based classification of glycoside hydrolases, *Curr. Opin. Struct. Biol. 7*, 637−644.
4. Tsukamoto, A., Kimura, K., Ishii, Y., Takano, T., and Yamane, K. (1988) Nucleotide sequence of the maltohexaose-producing amylase gene from an alakalophilic *Bacillus* sp.#707 and structural similarity to liquefying type α-amylases, *Biochem. Biophys. Res. Commun. 151*, 25−31.
5. Taniguchi, H. (1986) Plant α-amylases, in *Amylase* (Nakamura, M., Ed.) pp 168−170, Gakkai-Shuppan Center, Tokyo (in Japanese).
6. Bird, R., and Hopkins, R. H. (1953) The action of some α-amylases on amylose, *Biochem. J. 56*, 86−99.
7. Greenwood, C. T., Macgregor, A. W., and Milne, E. A. (1965) Action pattern of broad bean α-amylase, *Arch. Biochem. Biophys. 112*, 466−470.
8. Kadziola, A., Abe, J., Svensson, B., and Haser, R. (1994) Crystal and molecular structure of barley α-amylase, *J. Mol. Biol. 239*, 104−21.
9. Andre, G., Buleon, A., Haser, R., and Tran, V. (1999) Amylose chain behavior in an interacting context. III. Complete occupancy of the AMY2 barley α-amylase cleft and comparison with biochemical data, *Biopolymers 50*, 751−62.
10. Kimura, K., Tsukamoto, A., Ishii, Y., Takano, T., and Yamane, K. (1988) Cloning of a gene for maltohexaose producing amylase of an alkalophilic *Bacillus* and hyper-production of the enzyme in *Bacillus subtilis*, *Appl. Microbiol. Biotechnol. 27*, 372−7.
11. Nakamura, A., Haga, K., and Yamane, K. (1994) Four aromatic residues in the active center of cyclodextrin glucanotransferase from alkalophilic *Bacillus* sp. 1011: effects of replacements on substrate binding and cyclization characteristics, *Biochemistry 33*, 9929−36.
12. Otwinowski, Z., and Minor, W. (1997) in *Processing of X-ray Diffraction Data Collected in Oscillation Mode* (Carter, Jr., C. W., and Sweet, R. M., Eds.) Methods in Enzymology, 276, Macromolecular Crystallography, part A, pp 307−26, Academic Press, New York.
13. Brünger, A. T., Adams, P. D., Clore, G. M., DeLano, W. L., Gros P, Grosse-Kunstleve, R. W., Jiang, J. S., Kuszewski, J., Nilges, M., Pannu, N. S., Read, R. J., Rice, L. M., Simonson, T., and Warren, G. L. (1998) Crystallography & NMR system: A new software suite for macromolecular structure determination, *Acta Crystallogr. D54*, 905−21.
14. Machius, M., Declerck, N., Huber, R., and Wiegand, G. (2003) Kinetic stabilization of *Bacillus licheniformis* α-amylase through introduction of hydrophobic residues at the surface, *J. Biol. Chem. 278*, 11546−53.
15. Laskowski, A. R., MacArthur, M. W., Moss, D. S., and Thornton, J. M. (1993) PROCHECK: a program to check the stereochemical quality of protein structures, *J. Appl. Crystallogr. 26*, 283−291.
16. Gilson, M. K., Sharp, K. A., and Honig, B. H. (1987) Calculating the electrostatic potential of molecules in solution, *J. Comput. Chem. 9*, 327−35.
17. Honig, B., Sharp, K., and Yang, A. (1993) Macroscopic models of aqueous solutions: biological and chemical applications, *J. Phys. Chem. 97*, 1101−9.
18. Narimasa, S. (1973) A thermophilic extracellular α-amylase from *Bacillus licheniformis*, *Arch. Biochem. Biophys. 155*, 290−8.
19. Pfueller, S. L., and Elliott, W. H. (1969) The extracellular α-amylase of *Bacillus stearothermophilus*, *J. Biol. Chem. 244*, 48−54.
20. Matsuura, Y., Kusunoki, M., Harada, W., and Kakudo, M. (1984) Structure and possible catalytic residues of Taka-amylase A, *J. Biochem. (Tokyo) 95*, 697−702.
21. Machius, M., Declerck, N., Huber, R., and Wiegand, G. (1998) Activation of *Bacillus licheniformis* α-amylase through disorder→order transition of the substrate-binding site mediated by a calcium-sodium-calcium metal triad, *Structure 6*, 281−92.
22. Suvd, D., Fujimoto, Z., Takase, K., Matsumura, M., and Mizuno, H. (2001) Crystal structure of *Bacillus stearothermophilus* α-amylase: possible factors determining the thermostability, *J. Biochem. (Tokyo) 129*, 461−8.
23. Fujimoto, Z., Takase, K., Doui, N., Momma, M., Matsumoto, T., and Mizuno, H. (1998) Crystal structure of a catalytic-site mutant α-amylase from *Bacillus subtilis* complexed with maltopentaose, *J. Mol. Biol. 277*, 393−407.
24. Dauter, Z., Dauter, M., Brzozowski, A. M., Christensen, S., Borchert, T. V., Beier, L., Wilson, K. S., and Davies, G. J. (1999) X-ray structure of novamyl, the five-domain "maltogenic" α-amylase from *Bacillus Stearothermophilus*: maltose and acarbose complexes at 1.7Å resolution, *Biochemistry 38*, 8385−92.
25. Harata, K., Haga, K., Nakamura, A., Aoyagi, M., and Yamane, K. (1996) X-ray structure of cyclodextrin glucanotransferase from alkalophilic *Bacillus* sp.1011. Comparison of two independent molecules at 1.8Å resolution, *Acta Crystallogr. D52*, 1136−45.
26. Mosi, R., Sham, H., Uitdehaag, J. C. M., Ruiterkamp, R., Dijkstra, B. W., and Withers, S. G. (1998) Reassessment of acarbose as a transition state analogue inhibitor of cyclodextrin glycosyltransferase, *Biochemistry 37*, 17192−8.
27. Haga, K., Kanai, R., Sakamoto, O., Aoyagi, M., Harata, K., and Yamane K. (2003) Effects of essential carbohydrate/aromatic stacking interaction with Tyr100 and Phe259 on substrate binding

of cyclodextrin glycosyltransferase from alkalophilic *Bacillus* sp. 1011, *J. Biochem. (Tokyo) 134*, 881−91.
28. Brzozowski, A. M., Lawson, D. M., Turkenburg, J. P., Bisgaard-Frantzen, H., Svendsen, A., Borchert, T. V., Dauter, Z., Wilson, K. S., and Davies, G. J. (2000) Structural analysis of a chimeric bacterial α-amylase. High-resolution analysis of native and ligand complexes, *Biochemistry 39*, 9099−107.
29. Qian, M., Haser, R., Buisson, G., Duee, E., and Payan, F. (1994) The active center of a mammalian α-amylase. Structure of the complex of a pancreatic α-amylase with a carbohydrate inhibitor refined to 2.2-Å resolution, *Biochemistry 33*, 6284−94.
30. Kandra, L., Gyemant, G., Remenyik, J., Hovanszki, G., and Liptak, A. (2002) Action pattern and subsite mapping of *Bacillus licheniformis* α-amylase (BLA) with modified maltooligosaccharide substrates, *FEBS Lett. 518*, 79−82.
31. Maeda, I., Kiribuchi, S., and Nakamura, M. (1978) Digestion of barley starch granules by the combined action of α- and *β*-amylases purified from barley and barley malt, *Agric. Biol. Chem. 42*, 259−67.
32. Bak-Jensen, K. S., Andre, G., Gottschalk, T. E., Paes, G., Tran, V., and Svensson, B. (2004) Tyrosine 105 and threonine 212 at outermost substrate binding subsites −6 and +4 control substrate specificity, oligosaccharide cleavage patterns, and multiple binding modes of barley α-amylase 1, *J. Biol. Chem. 279*, 10093−102.

BI048489M